Available online at www.sciencedirect.com
SCIENCE DIRECT®
ELSEVIER
Journal of Magnetism and Magnetic Materials 281 (2004) 318–325
Journal of magnetism and magnetic materials
www.elsevier.com/locate/jmmm

The effect of Ho-doping and Ho-adding on electronic transport and magnetic properties of $La_{0.67}Ca_{0.33}MnO_3$

R.L. Zhang[a,*], Y. Feng[b], W.H. Song[a], J.M. Dai[a], Y.Q. Ma[a], J.J. Du[a], Y.P. Sun[a,1]

[a] *Key Laboratory of Materials Physics, Institute of Solid State Physics, Chinese Academy of Sciences, Hefei 230031, PR China*
[b] *Northwest Institute for Nonferrous Metal Research, P.O. Box 51, Xi'an, Shanxi 710016, PR China*

Received 19 April 2003; received in revised form 11 November 2003

Available online 7 June 2004

Abstract

The effect of Ho-doping and Ho-adding on the electronic transport and magnetic properties of melt-processed $La_{0.67}Ca_{0.33}MnO_3$ (LCMO) is investigated by resistivity and AC susceptibility measurement. For Ho-addition of 1 mol% LCMO sample (Ho-LCM), its magnetic transition temperature T_c and metal–insulator (M–I) transition temperature T_p are enhanced about 70 K compared with Ho-free LCMO sample. However, for Ho-doping of 3 mol% LCMO sample (Ho-doping LCM), both T_c and T_p are reduced about 35 K. We give a reasonable explanation in terms of structural changes (bond distance and bond angle) gained from the XRD refinement. The nanoscale Ho distribution is consistent with the magnetic inhomogeneity induced MR which is verified by the double peaks in AC susceptibility χ'' and the drop of $\chi'(T)$ curve below T_c. The mechanism of transport of all the samples is discussed.

PACS: 71.27.+a; 75.30.Vn; 71.30.+h

Keywords: Electronic transport and magnetic properties; Double exchange mechanism; XRD refinement; Lattice constants; Magnetic inhomogeneity

1. Introduction

The discovery of colossal magnetoresistance (CMR) in perovskite maganese oxides $R_{1-x}A_xMnO_3$ (where R is a trivalent rare-earth element and A is a divalent metal element such as Ca, Sr, Ba, Pb, etc.) has generated a considerable interest because of their various electronic, magnetic and structural properties and potential applications [1–7]. The spin structure and structural properties has long been correlated via the double exchange (DE) mechanism, i.e., the hoping of e_g electrons between Mn^{3+} and Mn^{4+} ions mediated by oxygen anions. Except for DE mechanism, Jahn–Teller electron–phonon coupling [8–10] arising from the deformation of the $Mn^{3+}O_6$ octahedra due to Jahn–Teller effect and the phase separation (PS) [11] also play an important role, Despite the reason for the existence of the PS state is

*Corresponding author. Tel.: +86-551-559-1436; fax: +86-551-559-1434.
E-mail addresses: rlzhang@issp.ac.an (R.L. Zhang), ypsun@issp.ac.cn (Y.P. Sun).
[1] Also for correspondence.

0304-8853/$ - see front matter © 2004 Elsevier B.V. All rights reserved.
doi:10.1016/j.jmmm.2004.04.121

not yet well understood, theoretical and experimental results found that the competition between different phases is very sensitive to the particular kind of disorder in the compound such as A- or B-site disorder, grain-size effect or intragranular strain [11–14], which lead to different transport properties and thus CMR effect.

Due to the difference in valence and size, different ions doping in $LaMnO_3$ could produce different effects, In the system of $La_{1-x}Ca_xMnO_3$, $x = 1/3$ is the most favorable doping which have a higher Curie temperature T_c and larger MR. At the same time T_c varies sensitively with varied chemical pressure, especially by introducing trivalent rare earth ions with different sizes into the perovskite structure [15–18], without varying the proportion of Mn^{3+} and Mn^{4+}. The doping changes the structural parameters which directly influences the e_g electrons hoping between Mn ions. The connectivity between grains enhances spin polarization between the adjacent grains through perovskite grain boundary (GB) region [19,20], because in ferromagnetic-metal mixture, the negative magnetoresistance (MR) effect originates from the spin-dependent scattering at the boundaries of the non-aligned magnetic grains. However, for bulk ceramic material, nearly 100% spin polarization remains an intriguing problem both for technological and scientific point of view. Therefore, the enhanced spin polarization is significant to investigate the structural MR at $T_c \approx T_{IM}$ (metal–insulator transition) in charge transport across the interface of the GB [21].

The melt-processed $La_{0.67}Ca_{0.33}MnO_3$ (Ho-free LCMO) has improved GB. In this work, the chemical pressure by doping Ho and adding Ho was studied through XRD refinement (which gives bond distance of Mn–O and bond angle of Mn–O–Mn); electric transport (zero field and low fields) and AC susceptibility measurements. We observed that T_c was nearly 70 K higher in Ho-LCM than that in Ho-free LCMO, but was nearly 35 K lower in Ho-doping LCM sample. Pradhan et al. [21] attributed this phenomenon to the opening of new conduction channels blocked at GB. In this article, a reasonable explanation is given based on the changes of structural parameters gained from Rietveld refinement of X-ray powder diffraction. The nanoscale Ho distribution is consistent with the magnetic inhomogeneity induced MR and this inhomogeneity can be verified from the double peaks appeared in the AC susceptibility imaginary part curve $\chi''(T)$ in the Ho-LCM sample and also the drop of χ' magnitude below T_c.

2. Experiment

$La_{0.67}Ca_{0.33}MnO_3$ (LCMO); $La_{0.64}Ho_{0.03}Ca_{0.33}MnO_3$ (Ho-doping LCM) and 1 mol% Ho addition to LCMO (Ho-LCM) samples were prepared by melt processing technique [22]. The samples were fully melt processed at $\sim$1600–1620°C and annealed in O_2. The X-ray powder diffraction was performed using a Philips PW 1700 X-ray diffractometer with Cu K_α radiation and was refined using a standard Rietveld technique [23]. Temperature dependence of resistivity for all the samples was measured by a standard four-probe method from 20 to 350 K. The AC susceptibility measurement was carried out by means of a sensitive mutual-inductance method operating at 1 kHz and a driven field of 0.15 G. The MR ratio is defined as $MR = (\rho_0 - \rho_H)/\rho_H * 100\%$. ρ_0 and ρ_H are the resistivity at zero field and applied field, respectively.

3. Results and discussion

X-ray powder diffraction at room temperature displayed in Fig. 1 indicates that all the samples are of single phase and the diffraction pattern can be indexed by orthorhombic lattice with space group Pbnm. The structural parameters were refined by the standard Rietvelt technique [23]. The results were listed in Table 1 where the lattice constants (a, b and c) of the doped samples are all larger than that of the Ho-free LCMO. However, the average Mn–O bond length of Ho-LCM is much smaller (except one Mn–O2) and the bond angle of Mn–O–Mn is much larger than that of LCMO. For Ho doping sample, it is of different case, the average Mn–O bond distance is longer (with only one Mn–O2 shorter) but the angle of Mn–O–Mn is smaller (except for one of the angles)

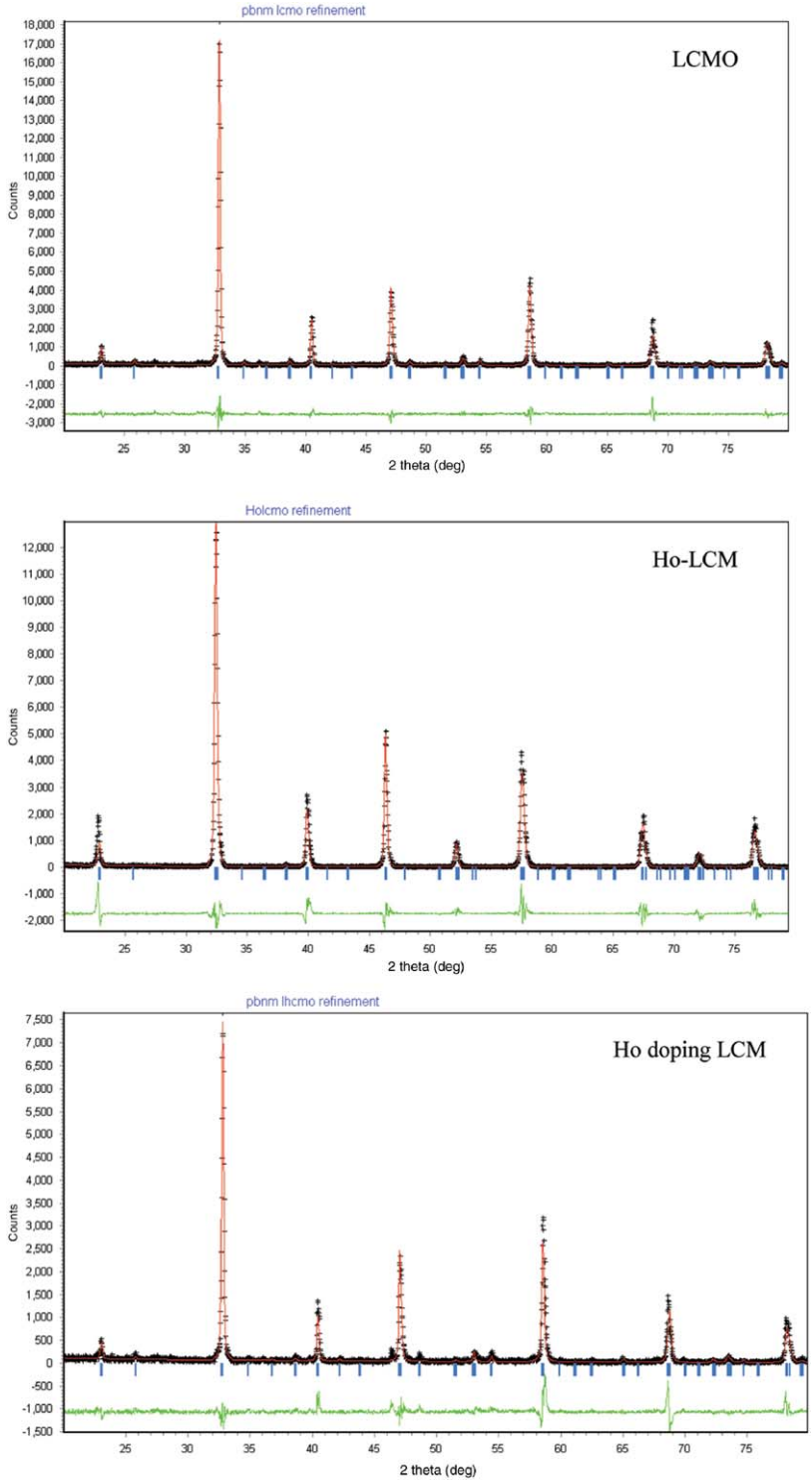

Fig. 1. XRD refinement of LCMO, Ho doping and Ho addition samples. Crosses indicate the experimental data and the calculated profile is the continuous line overlying them. The lowest curve shows the difference between experimental and calculated pattern. The vertical bars indicated the expected reflection positions.

Table 1
The structural parameters of all the samples from XRD refinement

Parameters	LCMO	Ho doping LCMO	Ho addition LCMO
a (Å)	5.4690	5.4692	5.5869
b (Å)	5.4568	5.4569	5.5574
c (Å)	7.7044	7.7057	7.8979
v (Å^3)	229.92	229.98	245.22
Mn–O1 (Å)	1.9470	1.9640	1.8650
Mn–O2 (Å)	1.9310	2.1360	1.6280
Mn–O2 (Å)	1.9770	1.8780	1.9780
Mn–O1–Mn (°)	163.16	164.61	167.79
Mn–O2–Mn (°)	162.56	157.50	170.83

than that of Ho-free sample. These changes in structure can be used to explain the transport proprieties mentioned below. It is well known that the tolerance factor t ($t = (r_A + r_O)/\sqrt{2}(r_B + r_O)$ (where r_i (i = A, B, or O) represents the average ionic size of each element). As t is close to 1, the cubic perovskite structure is realized. As r_A decreases, t also does, the lattice structure transforms to the rhombohedral ($0.96 < t < 1$) and then to the orthorhombic structure ($t < 0.96$), in which the bending of B–O–B bond and the deviation of the bond angle from 180° increase. Such structural transition has been confirmed by Sr- and Ba-doping system [24,25]. For our experiment, the ionic radii of La^{3+} and Ho^{3+} is 1.15 and 0.97 Å, respectively, and the substitution of smaller Ho^{3+} ions for larger La^{3+} leads to the tolerance factor to be $0.96 < t < 1$ and the structure to be orthorhombic. From Table 1, one may notice that the lattice parameters change a lot for Ho-add sample which indicates that Ho goes into the lattice (Ho is in the bulk). The extra Ho will cause Mn and oxygen vacancies in the crystal, which could be verified by the increase in cell volume for Ho-add sample compared with Ho-free sample.

Fig. 2 shows the temperature dependence of resistivity of LCMO, Ho doping and Ho-LCM samples at zero field and an applied field. All samples undergo a sharp transition at T_{IM} (metal–insulator transition temperature), which coincides well with the Curie transition temperature T_c (T_c can be defined from the AC susceptibility measurement). The paramagnetic–ferromagnetic (PM–FM) transition can be clearly seen in the temperature dependence of AC susceptibility plotted in the inset (a) of Fig. 2. In the ρ–T curve, the melt-processed LCMO exhibits a sharp T_c at $\sim$261 K which is enhanced compared with that of sintered LCMO. It was explained due to the opening of new conduction channels blocked at GB with improved grain boundaries for the melt-processed sample [19,20]. Compared with Ho-free LCMO, T_c of Ho-LCM (1 mol% Ho addition to LCMO) is increased $\sim$70 K and T_c of Ho-doping LCM is decreased $\sim$35 K. This kind of variation of T_c can be explained reasonably by the results of XRD refinement shown in Fig. 1 and Table 1. The smaller Mn–O distance and larger Mn–O–Mn angle in Ho adding LCMO lead to the enhancement of the bandwidth and the mobility of e_g electrons, the DE interaction is improved and the Curie temperature T_c increased in terms of DE model. However, for Ho doping sample, it is of the different case. The average length of Mn–O is larger and one of the angles of the Mn–O–Mn is larger too. These contrast cases compete with each other, which finally makes the longer bond distance and the smaller Mn–O–Mn angle to be prior, leading to the decreased DE interaction. Hence, both T_{IM} and T_c decreased in terms of DE model. It is clear that the Ho added material is much more metallic because of the increased bond angles and decreased bond distance. Therefore, it is suggested that the introduction of the second metallic phase with nanoscale (such as Ho here) to the CMR parent phase may be a valuable method enhancing the IM transition temperature and MR value.

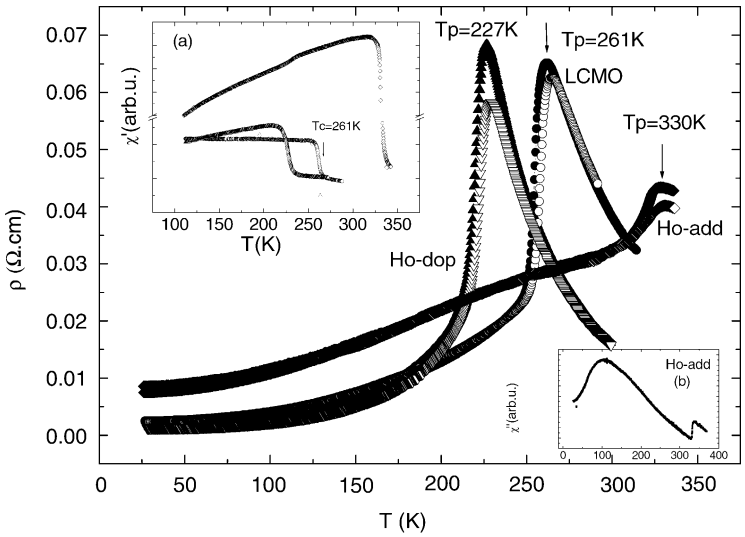

Fig. 2. Temperature dependence of the resistivity for all the samples in zero field and an applied field of 0.32 T. The inset (a) is the temperature dependence of AC susceptibility χ'. Inset (b) is the temperature dependence of AC susceptibility imaginary part χ'' of Ho-LCM sample.

Fig. 3 shows the temperature dependence of MR at a magnetic field of 0.32 T. It shows that the highest MR value of all the samples is achieved near T_{IM}. The CMR effect that occurs near T_c is associated with bulk and it occurs as the spins align and so the mobility of carriers increases. For the LCMO sample, the MR collapses rapidly below T_c indicating that the sample has a sharp phase boundary between ferromagnetic metallic (FMM) and charge ordering (CO) state [21]. However, a substantial MR remains at the low temperature for Ho-LCM. The field dependence of resistance ($R-H$) curve at room temperature (310 K) of Ho-LCM is plotted in the inset of Fig. 3, in which it displays a remarkable MR at room temperature. The low temperature MR is associated with grain boundaries and is caused by spin-dependent tunneling between grains, which indicates the FM and CO state remains coexistent almost all over the measured temperature region exhibiting the percolative conduction through metallic regions embedded in the insulating matric [21]. These results have been verified by the STM image shown in Ref. [21].

In order to verify the magnetic inhomogeneity caused by Ho addition, the temperature dependence of AC susceptibility imaginary part $\chi''(T)$ of Ho addition sample is measured as shown in the inset (b) of Fig. 2. It displays that Ho addition sample exhibits double peaks. For homogeneous samples, the temperature of the peak observed in $\chi''(T)$ is in agreement with the temperature of resistivity peak (T_p). However, for inhomogeneous samples, $\chi''(T)$ always shows multiple peaks [26]. Hence, the double peaks of $\chi''(T)$ in Ho-LCM sample indicates that the magnetic inhomogeneity is formed by Ho addition. Furthermore, the feature of $\chi'(T)$ curve also illustrates that it is not uniform FM in the Ho doping and Ho addition samples at the temperature region of $T < T_c$, but it is uniform FM in LCM sample. Therefore, the high temperature MR is considered to originate from the magnetic scattering due to the Ho addition, because magnetic inhomogeneity induces local strain, which will be discussed elsewhere in detail.

To understand the electric transport mechanism, the temperature dependences of the electrical resistivity data under zero field and applied field are fitted according to the small polaron hopping model, $\rho(T) \propto T\exp(E_0/kT)$ [27], thermally activated model, $\rho(T) \propto \exp(E_0/kT)$ and variable

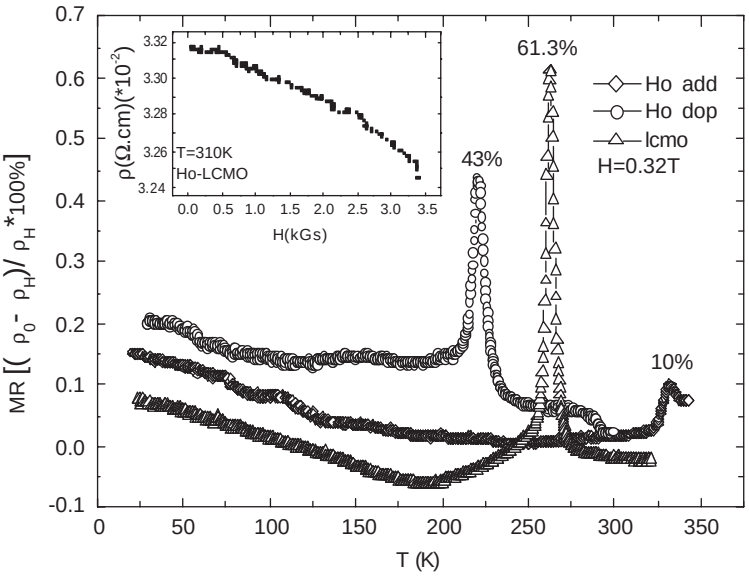

Fig. 3. Temperature dependence of MR defined as $\mathrm{MR} = [(\rho_0 - \rho_H)/\rho_H] \times 100\%$. The inset is $R-H$ curve at room temperature for Ho-LCM sample.

range hopping model, $\rho(T) \propto \exp[(T_0/T)^{\alpha}]$ [28], respectively. From the fitted results shown in Fig. 4, it is found that the resistivity data of LCMO and Ho-doping LCM can be well described by Mott's three-dimensional variable range hopping expression: $\rho(T) = \rho_0 \exp[(T_0/T)^{1/4}]$ at the high temperature region above T_p where T_0 is a characteristic temperature related to the density of states in the vicinity of the Fermi energy $N(E_F)$ and the localization length ζ, i.e., $k_B T_0 \approx 21/[\zeta^3 N(E_F)]$. For Ho-LCM sample, the experimental data can be fitted according to the small polaron model as shown in the inset of Fig. 4. That is to say, the electronic transport mechanism is changed when Ho is added into the LCMO sample. On the other hand, the transport mechanism transferred from variable range hopping in Ho-free sample to small polaron model in Ho-add samples perhaps indicates the better crystal quality of the latter caused by the lattice expansion and increase of the bond angles.

The same work is done for the temperature dependence of resistivity at the temperature region of $T < T_p$ using $\rho(T) = \rho_0 + AT^{\alpha}$ [29]. The results are shown in Fig. 5, we can see $\rho(T)$ lined well with $T^{2.7}$ for Ho-free LCM under zero field and an

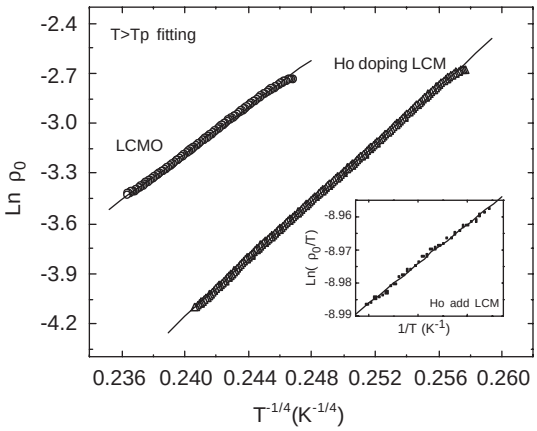

Fig. 4. Plot of $\ln \rho$ against $1/T^{1/4}$ of the resistivity data for LCMO and Ho-doping LCMO. The inset is the plot of $\ln(\rho/T)$ against $1/T$ of resistivity data for Ho-LCM.

applied field. Here ρ_0 is the resistivity due to the domain boundaries and other temperature-independent scattering mechanisms and the $AT^{2.7}$ term is an empirical fitting to the data which represents a combination of electron–electron, electron–phonon and electron–magnon scattering, all of these are expected to be significant in this system.

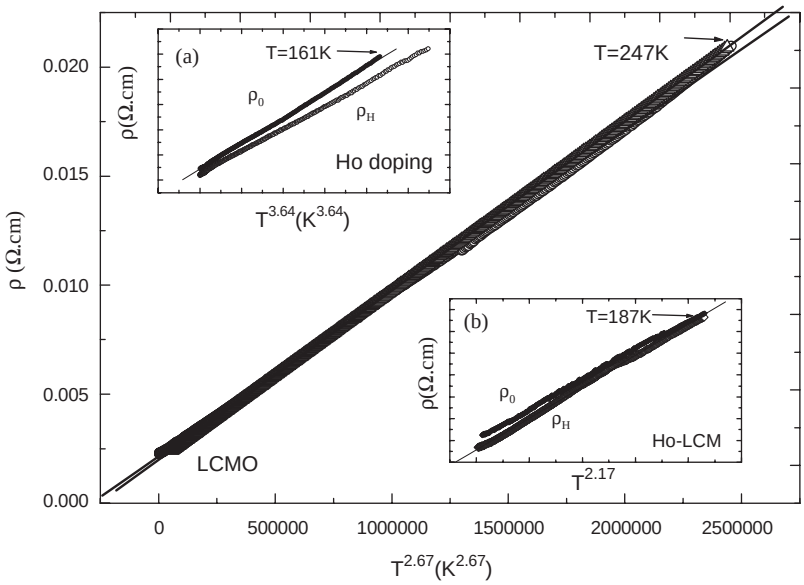

Fig. 5. Plot of ρ against $T^{2.7}$ of the resistivity data at $T < T_p$ for LCMO. Inset (a) is plot of ρ against $T^{3.6}$ for Ho doping sample and inset (b) is the plot of ρ against $T^{2.2}$ for Ho-LCM.

The temperature dependence of Ho-doping LCM is fit well by $AT^{3.6}$ as shown in the inset (a) of Fig. 5, which is near the $AT^{4.5}$ as suggested by Kubo and Ohata [30] based on calculation of electron–magnon scattering. However, the resistivity data of Ho addition sample was fit well by $AT^{2.2}$ (see inset b of the Fig. 5), which can also be thought to be the combination of electron–electron, electron–phonon and electron–magnon scattering. The doped samples have different transport mechanism from that of the LCMO and the lower α-value of Ho-LCM than that of LCMO also indicates the magnetic inhomogeneity induced by Ho adding, which is another proof of inhomogenety-induced MR at low temperatures.

4. Conclusions

In summary, the crystal structure, electric transport, magnetic properties and MR effect of melt-processing LCMO, Ho-doping LCM and Ho-LCM are investigated systematically and a reasonable explanation is suggested based on the viewpoint of structural changes. The average (Mn–O) bond length decreases and average $\langle$Mn–O–Mn$\rangle$ bond angle increases for Ho-LCM sample. In contrasted to Ho-LCM sample, the average (Mn–O) bond length increases and average $\langle$Mn–O–Mn$\rangle$ bond angle decreases for Ho-doping LCMO sample compared with the free-Ho LCMO sample. The enhanced T_c for Ho-LCM is ascribed to the enhanced double-exchange interaction due to the reduced (Mn–O) bond length and the increased $\langle$Mn–O–Mn$\rangle$ bond angle induced by nanoscale Ho distribution within LCMO. From the discussion, the introduction of Ho into LCMO drastically enhanced MR and increased T_c, which seems to be a common feature for CMR materials. It will be helpful method to search for CMR material with higher T_c and larger MR. The magnetic inhomogeneity induced by Ho addition was also verified by double peaks of the AC susceptibility $\chi''(T)$ measurement, $\chi'(T)$ curve and the fitting of $\rho(T)$ curve. This inhomogeneity may induce additional MR and open conduction channels at the same time.

Acknowledgements

This work is supported by the National Key Basic Research under contract No. 001CB610604, and the National Nature Science Foundation of China under contract No. 10174085, 10374033, Anhui Province NSF Grant No. 00046115, 03046201 and the Fundamental Bureau Chinese Academy of Sciences.

References

[1] R. von Helmolt, J. Wecker, B. Holzapfel, L. Schultz, K. Samwer, Phys. Rev. Lett. 71 (1993) 2331.
[2] S. Jin, T.H. Tiefel, M. McCormack, R.A. Fastnacht, R. Ramesh, L.H. Chen, Science 264 (1994) 413.
[3] G.Q. Gong, C. Canedy, G. Xiao, J.Z. Sun, A. Gupta, W.J. Gallagher, Appl. Phys. Lett. 67 (1995) 1783.
[4] G.C. Xiong, Q. Li, H.L. Ju, S.N. Mao, L. Senapati, X.X. Xi, R.L. Greene, T. Venkatesan, Appl. Phys. Lett. 66 (1995) 1427.
[5] A. Asamitsu, Y. Moritomo, Y. Tomioka, T. Arima, Y. Tokura, Nature (London) 373 (1995) 407.
[6] V. Caignaert, A. Maignan, B. Raveau, Solid State Commun. 95 (1995) 357.
[7] J.M.D. Coey, M. Viret, S. von Molnar, Adv. Phys. 48 (1999) 167.
[8] A.J. Millis, P.B. Littlewood, B.I. Shraiman, Phys. Rev. Lett. 74 (1995) 5144.
[9] A.J. Millis, B.I. Shraiman, R. Mueller, Phys. Rev. Lett. 77 (1996) 175.
[10] A.J. Millis, Phys. Rev. B 53 (1996) 8434.
[11] M. Uehara, S. Mori, C.H. Chen, S.-W. Cheong, Nature 399 (1999) 560.
[12] T. Kimura, Y. Tomioka, R. Kumai, Y. Okimoto, Y. Yokura, Phys. Rev. Lett. 83 (1999) 3940.
[13] R. Mahendiran, M. Herieu, A. Maignan, C. Martin, B. Raveau, Solid State Commun. 114 (2000) 429.
[14] P. Levy, F. Parisi, G. Polla, D. Vega, G. Leyva, H. Lanza, R.S. Freitas, L. Ghivelder, Phys. Rev. B 62 (2000) 6437.
[15] H.Y. Hwang, S.W. Cheong, P.G. Radaell, M. Marezio, B. Batlogg, Phys. Rev. Lett. 75 (1995) 914;
H.Y. Hwang, S.W. Cheong, N.P. Ong, Phys. Rev. Lett. 77 (1996) 2041.
[16] S. jin, T.H. Tiefel, M. McCromack, R.A. Fastnatch, Science 264 (1994) 413.
[17] J.M.D. Coey, M. Viret, L. Ranno, K. Ounadjela, Phys. Rev. Lett. 75 (1995) 3910.
[18] K. Khazeni, Y.X. Jia, L. Lu, V.H. Crespi, M.L. Cohen, A. Zettl, Phys. Rev. Lett. 76 (1996) 295.
[19] A.K. Pradhan, B.K. Roul, J.G. Wen, Z.F. Ren, Appl. Phys. Lett. 76 (1996) 4042.
[20] A. de Andres, M. Gracia-Hernandez, J.L. Martinez, C. Prieto, Appl. Phys. Lett. 74 (1999) 3884.
[21] A.K. Pradhan, B.K. Roul, Y. Feng, Appl. Phys. Lett. 78 (2001) 11.
[22] A.K. Pradhan, B.K. Roul, J.G. Wen, Z.F. Ren, Appl. Phys. Lett. 76 (1996) 4042.
[23] D.B. Wiles, R.A. Young, J. Appl. Crystallogr. 14 (1981) 149.
[24] P.G. Radaelli, M. Marezio, H.Y. Hwang, S.-W. Cheong, B. Batlogg, Phys. Rev. B 54 (1996) 8992.
[25] R. Mallik, E.S. Reddy, P.L. Paulose, S. Majumdar, E.V. Sampathkumaran, J. Phys.: Condens. Matter 11 (1999) 4179.
[26] F.M. Araujo-Moreira, M. Rajeswari, A. Goyal, K. Ghosh, V. Smolyaninova, et al., Appl. Phys. Lett 73 (1998) 3456.
[27] G. Jakob, W. Westerberg, F. Martin, Phys. Rev. B 58 (1998) 14966.
[28] N.F. Mott, E.A. Davis, Electronic Processes in Non-Crystalline Solids, 2nd Edition, Clarendon Press, Oxford.
[29] J.M. De Teresa, M.R. Ibarra, J. Blasco, J. García, C. Marquina, P.A. Algarabel, Z. Arnold, K. Kamenev, C. Ritter, R. Von Helmolt, Phys. Rev. B 54 (1996) 1187.
[30] K. Kubo, N. Ohata, J. Phys. Soc. Jpn. 33 (1972) 21.